J. Am. Ceram. Soc., 71 [1] 42-49 (1988)

Atomistic Simulation of Defect Structures and Ion Transport in α-Fe_2O_3 and α-Cr_2O_3

C. RICHARD A. CATLOW

Department of Chemistry, University of Keele, Staffordshire ST5 5BG, England

JOHN CORISH and JOHN HENNESSY

Department of Chemistry, Trinity College, Dublin 2, Ireland

WILLIAM C. MACKRODT*

Imperial Chemical Industries plc, New Science Group, The Heath, Runcorn, Cheshire WA7 4QE, England

Computer-modelling techniques are applied to the calculation of defect formation and migration energies in α-Fe_2O_3 and α-Cr_2O_3: both electronic and lattice defects are considered. The results are used to predict Arrhenius energies for cation and anion migration in different composition and temperature regimes and show reasonable agreement with experimental data where these are available.

I. Introduction

THE transport of host lattice cations and anions through corundum-structured α-Fe_2O_3 and α-Cr_2O_3 plays a crucial role in the high-temperature corrosion of many commercially important alloys. Despite the evident implications for this and other processes, a knowledge of the defect structure and matter transport mechanisms in these materials remains obscure. The principal reason for this is that the two oxides are difficult to prepare in a sufficiently pure crystalline form, while their study is complicated further by the fact that they are mixed conductors in which charge may be transported by both electronic and ionic carriers. An additional complication is that the primary lattice disorder in these materials can arise either intrinsically or as a result of departures from stoichiometry, or from the presence of aliovalent impurities.

Early experimental work by Chang and Wagner[1] on naturally occurring single crystals of α-Fe_2O_3, in which they studied the effect of oxygen partial pressure on the self-diffusion of iron and the electrical conductivity, suggested that the material was predominantly an intrinsic semiconductor. More recent measurements of electrical conductivity made by Dieckmann[2] on material which was produced by the oxidation of a 99.998% pure iron substrate confirmed this view and indicated that conduction by electronic defects was virtually independent of the oxygen partial pressure at temperatures between 1273 and 1573 K. Hoshino and Peterson,[3] who studied the diffusion of iron in single crystals of α-Fe_2O_3 supplied by Cristal Tec (France), agreed with Chang and Wagner in deducing that the cations moved by an interstitial-type mechanism, but, in contrast to the earlier work,[1] concluded that oxygen vacancies, $V_O^{\cdot\cdot}$, and divalent interstitial ions, $Fe_i^{\cdot\cdot}$, were the predominant defects. Furthermore, their measured absolute diffusion rates and the observed dependence on both the temperature and partial pressure of oxygen all differed substantially from those reported by Chang and Wagner.[1] More recently Hoshio and Peterson[4] measured the cation self-diffusion coefficient, D^*_{Fe}, parallel to the c axis in single crystals of the same origin as those used by Chang and Wagner, as a function of temperature and p_{O_2}; they also studied the diffusion of a number of impurities in the same material. These new measurements confirmed the oxygen partial pressure dependence of D^*_{Fe} observed by Chang and Wagner[1] but the absolute value and the activation enthalpy for the self-diffusion process were much higher than had been measured previously.[1] These results suggest that the majority of the diffusion studies[1-4] have been carried out on samples in which the defect concentrations were controlled by impurities and that under such conditions the concentration of electronic carriers would be independent of the oxygen partial pressure. Atkinson and Taylor[5] have also reported measurements of D^*_{Fe} in α-Fe_2O_3 single crystals in the temperature range 981 to 1576 K and at unit oxygen activity and suggest that their data above 1173 K are characteristic of the pure material, whereas those at lower temperatures are influenced by the impurities present in their samples.

The early work on diffusion and other aspects of the defect structure of α-Cr_2O_3 has been reviewed extensively by Kofstad.[6] More recently Atkinson and Taylor[7] have studied the self-diffusion of Cr in α-Cr_2O_3 single crystals at temperatures of 1373 and 1573 K and for a range of oxygen activities. They conclude that the dependence on the oxygen partial pressure suggests that diffusion is effected by vacancies at high p_{O_2}; however, they also found a substantial contribution from diffusion along dislocations in the crystals.

In an attempt to clarify and understand what is, at present, an incomplete picture of the atomic disorder and associated volume transport in α-Fe_2O_3 and α-Cr_2O_3 we have carried out defect lattice simulations, similar to those used in previous studies of other transition metal oxides,[8-11] and here report formation energies of a variety of electronic and lattice defects and migration energies for a number of possible vacancy, direct interstitial, and interstitialcy mechanisms. Since departures from stoichiometry are expected to be important in the control of defect populations, at least in relatively pure crystals, the results of these calculations are then used to predict the defect structures which might be expected under both oxidizing and reducing atmospheres. Also reported is p_{O_2} dependence for the major defects.

II. Theoretical Methods

The calculations were performed using simulation methods related to the Mott-Littleton[12] procedure for noncubic crystals available in the HADES III[13] and CASCADE[14] codes, a discussion of the methodology of which is available elsewhere.[15] Prior to performing the defect calculations the position of all atoms in the unit cell and the cell dimensions were equilibrated (i.e., relaxed to zero force). The magnitudes of the displacements of all atoms from the experimental[16] to the equilibrated positions were small and the residual strains were also small — less than 10^{-3}. The defect calculations were then performed with inner, explicitly relaxed regions of between 100 and 120 ions, which is sufficiently large to ensure reliable results.

Fully ionic, shell model[17] potentials were used to describe the interionic forces in both crystals. The short-range potentials were obtained using the modified electron gas procedure developed by Mackrodt and Stewart.[18] The electronic densities for the Fe^{3+} and Cr^{3+} cations were obtained using the wave function for the free

Received November 11, 1986; approved June 24, 1987.
*Member, the American Ceramic Society.

Table I. Interionic Potentials

(*A*) Short-Range Parameters for Potential Form $V(r) = Ae^{-r/\rho} - Cr^{-6}$

Interaction	A ($\times 10^{-1}$ J·mol^{-1})	ρ (m^{-10})	C (kJ·mol^{-1}·m^{-60})	Range (m^{-10})
Fe^{3+}–Fe^{3+}	215.5	0.18546	1395.84	0.0–1.69337
	291.0	0.17531	234.79	1.69337–3.43965
	0.0	1.0	0.0	3.43895–∞
Fe^{3+}–O^{2-}	33.1	0.27828	563.80	0.0–1.7992
	38.4	0.27468	1851.26	1.7992–2.6459
	53.1	0.26112	389.60	2.6459–4.2334
	0.0	1.0	0.0	4.2334–∞
O^{2-}–O^{2-}	2.6	0.43934	37.02	0.0–1.7992
	8.4	0.36709	6800.43	1.7992–2.6459
	9.8	0.35609	5528.09	2.6459–4.2334
	0.0	1.0	0.0	4.2334–∞
Cr^{3+}–Cr^{3+}	155.8	0.19870	1775.70	0.0–2.1167
	9172.6	0.11579	−1265.00	2.1167–3.4395
	0.0	1.0	0.0	3.4395–∞
Cr^{3+}–O^{2-}	27.2	0.28694	161.48	0.0–1.3758
	35.1	0.27947	2202.62	1.3758–1.9579
	38.0	0.27395	1129.62	1.9579–2.6458
	52.0	0.26333	512.30	2.6458–4.02167
	0.0	1.0	0.0	4.02167–∞

(*B*) Shell Parameters

Ion	Y (e)	k (kJ·mol^{-1}·m^{-20})
Fe^{3+}	5.38	6281
Cr^{3+}	7.40	20201
O^{2-}	− 1.9740	1546

Note: All other ions were treated as unpolarizable.

ions developed by Clementi.[19] As the free O^{2-} ion is unstable, the electron density for this species was calculated by solving the Hartree-Fock equations for the species in the Madelung field appropriate to this ion in the crystal environment. In the calculation reported on the O^- substitutional, we used the same short-range potential as for the O^{2-} ion. The numerical potentials given by the electron gas calculation were fitted to the simple analytical function

$$V(r) = Ae^{-r/\rho} - Cr^{-6}$$

A single function of this type does not adequately reproduce the calculated potentials, which were therefore divided into a number of ranges of internuclear separation, each with different potential parameters. The parameters with their appropriate ranges are given in Table I.

As there are no theoretical procedures for calculating shell model parameters, these were determined by least-squares fitting to the observed static[20] and high-frequency dielectric constants.[21] Both cations and anions were allowed to be polarizable.

In studying cation interstitialcy motion in α-Fe_2O_3, we found that the interionic potential discussed above showed excessive polarization of the cations. For this reason we developed an alternative model for α-Fe_2O_3 in which the cations are unpolarizable. The oxygen shell charge and spring constant were fitted to ε_0 and ε_∞, giving the parameters reported in Table II. This potential proved to be stable when used in calculations on interstitialcy migration; moreover, it led to negligible differences in the values calculated for the basic defect energies.

III. Results

(1) *Basic Defect Formation Energies*

In Table III we give the calculated energies for cation and anion vacancies and interstitials; both trivalent and divalent cation interstitials were considered. From these we obtain Schottky and Frenkel defect formation energies which are given in the same table as energies *per constituent defect*. For comparative purposes we also quote results[13,22] obtained for the isostructural α-Al_2O_3 crystal using the same theoretical procedures.

(2) *Electronic Defects*

Calculations were performed on (1) the Fe^{2+} substitutional, a model for the electron, polaron in this system, and (2) the O^- substitutional, the model for the hole, polaron. Our calculations found that it was more energetically favorable by at least 387 kJ·mol^{-1} to create a hole on the oxygen rather than the metal sublattice. Two calculations were performed in each case: first a conventional calculation in which the lattice was fully relaxed

Table II. Other Interionic Potentials*

(*A*) Short-Range Parameters for Potential Form $V(r) = Ae^{-r/\rho} - Cr^{-6}$

Interaction	A ($\times 10^{-1}$ J·mol^{-1})	ρ (m^{-10})	C (kJ·mol^{-1}·m^{-60})	Range (m^{-10})
Fe^{3+}–O^{2-}	10.7129	0.3578	0.0	0.0–3.50
	0.0	1.0	0.0	3.50–∞

(*B*) Shell Parameters

Ion	Y (e)	k_1 (kJ·mol^{-1}·m^{-20})	$k_2^\dagger$ ($\times 10^{-7}$ J·mol^{-1}·m^{-40})	$k_3^\dagger$ ($\times 10^{-7}$ J·mol^{-1}·m^{-60})
O^{2-}	−2.8057	1441	483	483

*List of parameters which differ from those in Table I and which refer to the potential in which the Fe^{3+} cation in α-Fe_2O_3 was made unpolarizable to calculate the energies for the interstitial-type migration.

†k_2 and k_3 are the coefficients of higher-order terms in the core-shell self energy; k_2 is the coefficient of the x^4 term, where x is the core-shell separation, and k_3 the coefficient of the x^6 term.

Table III. Calculated Defect Energies for the Basic Atomistic Defects

Defect	Defect energy of crystal ($kJ \cdot mol^{-1}$)		
	α-Fe_2O_3	α-Cr_2O_3	α-Al_2O_3†
V'''_m (cation vacancy)	5305	5244	5909
$V^{\cdot\cdot}_O$ (anion vacancy)	1962	1957	2102
$M_i^{\cdot\cdot\cdot}$ (cation interstitial)	−4139	−4050	−4540
O_i'' (anion interstitial)	−904	−923	−504
$M_i^{\cdot\cdot}$ (divalent cation interstitial)	−1562	−1537	
Cation Frenkel*	585	597	685
Anion Frenkel*	527	614	799
Schottky*,‡	427	407	497

*Energy per constituent defect. †Using the nonempirical potential of Ref. 13. ‡Estimated using calculated lattice energies in $kJ \cdot mol^{-1}$ per formula unit of −14 368 for α-Fe_2O_3 and −14 327 for α-Cr_2O_3.

Table IV. Calculated Lattice Energy Changes for the Formation of Electronic Defects

Electronic defect	Lattice energy of crystal ($kJ \cdot mol^{-1}$)	
	α-Fe_2O_3	α-Cr_2O_3
Hole (O^-) (small polaron)	1485	1508
Hole (O^-) (large polaron)	1556	1612
Electron (M^{2+}) (small polaron)	2775	2774
Electron (M^{2+}) (large polaron)	2870	2879
Hole (M^{4+}) (small polaron)	−3778	−3790
Hole (M^{4+}) (large polaron)	−3682	−3683

Table V. Values of Energies Required to Calculate Defect Energies

Parameter	Energy of crystal ($kJ \cdot mol^{-1}$)	
	α-Fe_2O_3	α-Cr_2O_3
Third ionization potential (M)	2961	2991
Second electron affinity (O)	−879	−879
O(2*p*) bandwidth	618	618
M(3*d*) bandwidth	≈97	≈97

Table VI. Formation Energies for Electronic Defects

Defect	Defect formation energy of crystal ($kJ \cdot mol^{-1}$)	
	α-Fe_2O_3	α-Cr_2O_3
Hole (small polaron)	606	629
Hole (large polaron)	367	423
Electron (small polaron)	−186	−217
Electron (large polaron)	−139	−160
Calculated band gap	182	207

around the substituted ion; we take the resulting energy as referring to the small polaron. In the second calculation only the shells were relaxed which, as discussed by Mackrodt,[23] provides a model for the structure of the large polaron. Results of the calculations are given in Table IV.

To estimate the small polaron formation energies we add to the lattice energy, here calculated by the simulation program, the appropriate ionization energy, i.e., the third ionization energy of the metal for the case of the electron states and the second electron affinity of oxygen in the case of the hole state; the values used for these quantities are reported in Table V. In calculating the large polaron formation energies as discussed by Mackrodt,[23] we subtract from the sum of the lattice energy term and the ionization energy (Table V) half the value of the appropriate bandwidth which is also reported in Table V. As these data are not available experimentally, the value for the O(2*p*) bandwidth was taken to be the same as the isostructural crystal α-Al_2O_3. By comparison with other transition metal oxides we would not expect the 3*d* bandwidths to be $\gtrsim$100 $kJ \cdot mol^{-1}$. The resulting energies are given in Table VI.

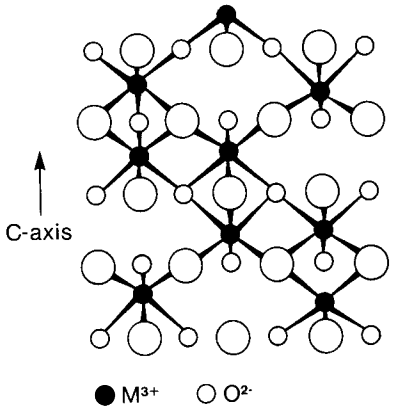

Fig. 1. Corundum structure.

The calculations suggest for both materials that the hole state is a large polaron and the electron a small polaron. By combining the two energies we obtain our estimate of the band gap which is given in Table VI.

(3) Defect Migration Energies

(A) Vacancy Motion: The corundum structure is shown in Fig. 1. James[22] has identified the following six saddle points for cation vacancy motion in this structure:

(i) The C1 configuration, in which a cation migrates along the *c* axis between two neighboring cation sites which share a common octahedral face. In the saddle point, shown in Fig. 2(*A*), the cation is at the centroid of the triangle of oxygen ions in the shared face.

(ii) The C2 configuration, in which the cation again migrates along *c*, but moves through an interstitial site. Two saddle point configurations were investigated: in the C2 configuration the migrating cation is in the centroid of the oxygen ion triangle as it leaves the MO_6 octahedron as shown in Fig. 2(*B*).

(iii) The C3 configuration relates to the same migration process as does the C2, but the migrating cation is at the interstitial site between the two cation lattice sites.

(iv) The C4 configuration is envisaged by examining the anion coordination which can be described in terms of a trigonal prismatic arrangement (see Fig. 2(*C*)) in which four of the apices are occupied by cations and two are vacant (i.e., intersitial sites). The cation jumps across the prism through an oxygen anion triangle as shown in the figure.

(v) The C5 configuration (Fig. 2(*D*)) relates to a jump in the *ab* plane through an interstitial site; for the saddle point we assume that the migrating ion is at the center of this site.

(vi) The C6 configuration (Fig. 2(*E*)) involves migration between nearest-neighbor cation sites and the migration vector has components both parallel and perpendicular to *c*. In the saddle point the migrating ion is assumed to be midway between the two sites.

Not all of these mechanisms will effect diffusion. Transport parallel to *c* can be effected by a combination of mechanisms for which the C1, C2, and C3 configurations are the saddle points. C5 can effect diffusion but only within the *ab* plane. Both C4 and C6 will effect diffusion with components both perpendicular and parallel to *c*.

The calculated activation energies for each of the six configurations are reported in Table VII, where they are compared with the values calculated by James[22] for α-Al_2O_3.

(B) Anion Migration: The following five mechanisms for anion diffusion have been proposed:[22]

(i) The A1 configuration is confined to the *ab* plane. The migrating anion moves between two oxygen sites in the anion triangle shared between two MO_6 octahedra as shown in Fig. 3(*A*).

(ii) The A2 configuration is similar to A1, but the anion trian-

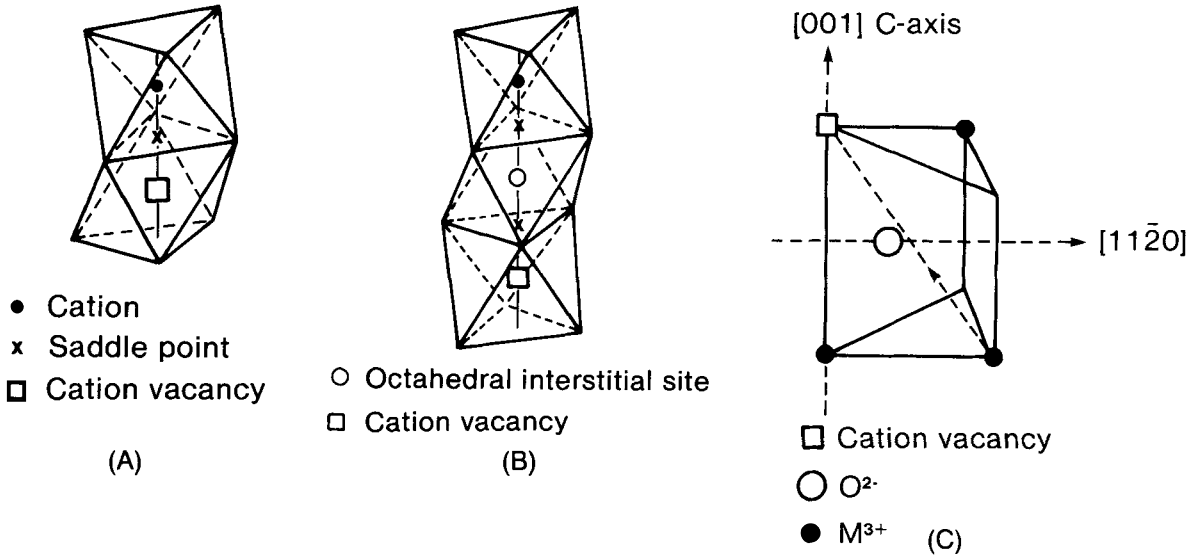

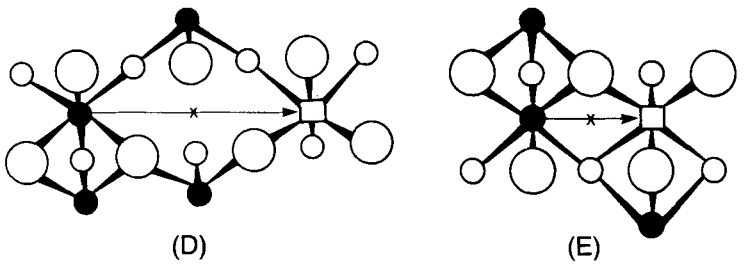

Fig. 2. Possible migration pathways for cation vacancy motion in the corundum structure. The various configurations are described in the text: (*A*) C1 configuration; (*B*) C2 configuration; (*C*) C4 configuration; (*D*) C5 configuration; (*E*) C6 configuration.

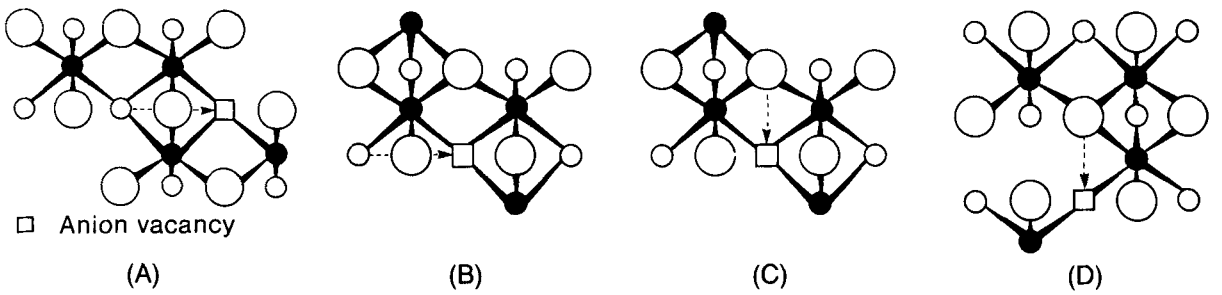

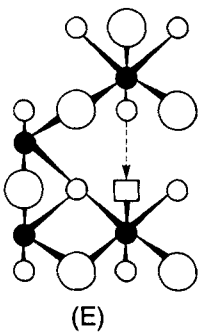

Fig. 3. Possible migration pathways for anion vacancy motion in the corundum structure. The various configurations are described in the text: (*A*) A1 configuration; (*B*) A2 configuration; (*C*) A3 configuration; (*D*) A4 configuration; (*E*) A5 configuration.

gle now lies between a filled cation site and an interstitial site, as shown in Fig. 3(*B*).

(iii) The A3 configuration in which the anion moves along a shared edge of two MO_6 octahedra and between two layers of anions, as shown in Fig. 3(*C*).

(iv) The A4 configuration is similar to the A3, but the shared edge now lies between an octahedron which contains a cation and one surrounding an interstitial site as shown in Fig. 3(*D*).

(v) The A5 configuration in which the migrating anion moves between anion layers across the body diagonal of an interstitial site as shown in Fig. 3(*E*).

Table VII. Calculated Diffusion Energies for Cation Vacancy Mechanisms

Mechanism	Diffusion energy of crystal (kJ·mol^{-1})		
	α-Fe_2O_3	α-Cr_2O_3	α-Al_2O_3*
C1	343	340	223
C2	171	169	140
C3	−10	−13	−7
C4	207	204	175
C5	870	863	981
C6	217	213	198

*Using the nonempirical potential of Ref. 13.

Table VIII. Calculated Diffusion Energies for Anion Vacancy Mechanisms

Mechanism	Diffusion energy of crystal (kJ·mol^{-1})		
	α-Fe_2O_3	α-Cr_2O_3	α-Al_2O_3*
A1	108	108	108
A2	255		586
A3	217	240	171
A4	262	245	467
A5	1009	1043	920

*Using the nonempirical potential of Ref. 13.

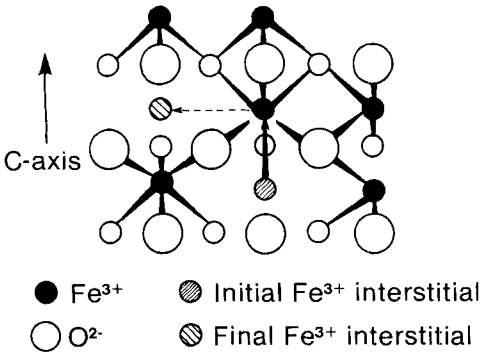

Fig. 4. I3 interstitialcy migration mechanism in the corundum structure.

In every case the saddle point is taken to be midway between the two anion sites involved in the mechanism. Again it should be noted that A1 and A2 configurations only effect transport in the *ab* plane, whereas A3, A4, and A5 effect isotropic diffusion, i.e., both parallel and perpendicular to *c*.

The calculated values for the anion activation energies are given in Table VIII, where they are again compared with the values calculated by James[22] for α-Al_2O_3.

(C) Interstitial Migration: As these calculations were computationally expensive, we confined our study of interstitial migration to cation motion, as there do not seem to be circumstances under which the movement of interstitial anions could contribute to transport in these materials.

We first investigated direct interstitial motion in which the migrating cation interstitial moves through an anion triangle between nearest-neighbor interstitial sites. High values of more than 970 kJ·mol^{-1} for α-Fe_2O_3 were obtained for the activation energies, and the mechanisms will not be considered subsequently.

There are several interstitialcy mechanisms in each of which the interstitial ion displaces a lattice cation into a neighboring interstitial site and itself occupies that cation site at the end of the mechanism.

These mechanisms thus involve two moving ions and are described as follows:

(i) The I1 configuration in which the interstitial ion moves in the *ab* plane to displace a lattice cation to the nearest interstitial site within that plane.

(ii) The I2 configuration, where the interstitial ion takes a longer jump with components both in the *ab* plane and in the *c* direction and the displaced lattice cation moves to the nearest interstitial site within its *ab* plane.

(iii) The I3 configuration, where the interstitial ion moves along the *c* axis toward a lattice cation which in turn is again displaced to the nearest interstitial site within its *ab* plane, as shown in Fig. 4.

(iv) The I4 configuration is again initiated by the motion of an ion in the *c* direction, but the displaced ion makes the longer jump with components in both the *ab* plane and the *c* direction.

To identify accurately a saddle point for interstitialcy motion the following procedure must be used. The first ion is fixed at a series of points along the approach direction to the lattice cation which is to be displaced while allowing that cation and the remainder of the lattice to relax in the energy minimization procedure. The resulting potential energy profile for the case of the I3 mechanism in α-Fe_2O_3 is shown in Fig. 5.

Detailed calculations were only performed for the case of the Fe^{3+} interstitial in α-Fe_2O_3. The computational expense of the calculation did not justify a study of Cr^{3+} in α-Cr_2O_3 as the results are expected to be very similar. We found that the I2 and I4 "midpoint" activation energies for α-Fe_2O_3 (i.e., the energies when the "fixed" ion in the calculation is halfway between the interstitial and the lattice site) were high, 1024 and 928 kJ·mol^{-1}, respectively, so that further calculations on these mechanisms were considered to be futile. A detailed profile was, however, determined for the I1 mechanism which shows an activation energy of 657 kJ·mol^{-1} while that for the I3 mechanism, as shown in Fig. 5, is 193 kJ·mol^{-1}.

Preliminary calculations for the interstitialcy movement of Fe^{2+} in α-Fe_2O_3 were also made. However, identification of the saddle point is difficult in this case as the process must involve transfer of an electron between the two migrating ions. Thus far we have no evidence that Fe^{2+} interstitialcy motion requires a lower activation energy than the interstitialcy motion of Fe^{3+} by the favored I3 mechanism.

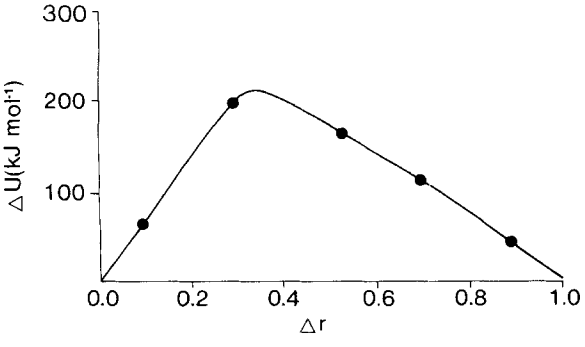

Fig. 5. Calculated potential energy profile for the I3 interstitialcy migration mechanism in α-Fe_2O_3. Δu is the activation energy and Δr the extent, in lattice units, of the displacement of the initial interstitial ion toward the lattice cation which it displaces.

IV. Discussion

Our calculations agree with experiment in giving formation energies for electronic defects that are substantially lower than those for the atomistic defects. In both materials we predict that the holes will be large polaron and the electrons small polaron species. At the quantitative level, we find reasonable agreement between the calculated band gap of 184 kJ·mol^{-1} for α-Fe_2O_3 and the experimental values of 228[1] and 209 to 236[24] kJ·mol^{-1} from electrical conductivity and 207 kJ·mol^{-1} from optical measurements.[24] The comparison for the case of α-Cr_2O_3 is apparently less satisfactory as the experimental estimate[25] gives a band gap of at least 348 kJ·mol^{-1} compared with our calculated result of 203 kJ·mol^{-1}. However, we consider that this discrepancy is explicable in terms of ligand field effects. On creating an electron polaron state by reducing M^{3+} to M^{2+}, in α-Fe_2O_3 we add an electron to the t_{2g} orbitals of the cation, whereas in α-Cr_2O_3 the electron will be added to the e_g orbitals. Since ligand field factors are ignored in our calculations, we should therefore correct the electron formation energy in α-Fe_2O_3 by $-\frac{2}{5}\Delta$ and that in α-Cr_2O_3 by $+\frac{3}{5}\Delta$, where Δ is the ligand field splitting energy of the cation in the oxide environment, and is $\approx$174 kJ·mol^{-1} for α-Fe_2O_3 and 290 kJ·mol^{-1} for α-Cr_2O_3.[26] Our corrected band gap for the former oxide would then be $\approx$ 116 kJ·mol^{-1}, which is now lower than the quoted experimental value. For α-Cr_2O_3 we obtain a corrected value of 377 kJ·mol^{-1}, which is now in much better agreement with experiment.[25]

The intrinsic atomistic defect formation energies are high, the lowest being that for Schottky disorder. With formation energies of 387 to 435 kJ·mol^{-1} per defect it is unlikely that intrinsic defect generation will ever be significant, and in practice defect populations may be taken as being due to compensation for impurities or to deviations from stoichiometry.

We now concentrate on the latter considering oxidation and then reduction of the oxides.

(1) Defect Structure and Energies in Oxidized Crystals

Oxidation takes place at high p_{O_2} by formation of holes which can be compensated by either oxygen interstitials or metal vacancies. In the former case the oxidation reaction is written as

$$O_2 \longrightarrow 2O_i'' + 4h^{\cdot} \tag{1}$$

for which the energy E_{ox} can be calculated as

$$E_{ox}^{O_i''} = E_D + 2E_{12} + 2E_{O_i''} + 4E_{h^{\cdot}} \tag{2}$$

where E_D is the dissociation energy of O_2 for which a value of 487 kJ·mol^{-1} is used; E_{12} is the sum of the first and second electron affinities of oxygen, for which we take the value of 792 kJ·mol^{-1}.[13] $E_{O_i''}$ and $E_{h^{\cdot}}$ are the formation energies of the oxygen interstitial and the large polaron hole, respectively; the values were taken from Tables III and IV. The resulting oxidation energies are 1731 and 1923 kJ·mol^{-1} for α-Fe_2O_3 and α-Cr_2O_3, respectively.

The corresponding reaction for oxidation with vacancy compensation is

$$O_2 + \tfrac{4}{3}M_M^{\times} \rightarrow \tfrac{4}{3}V_M''' + 4h^{\cdot} + \tfrac{2}{3}M_2O_3 \tag{3}$$

and the corresponding energy expression is

$$E_{ox}^{V_M'''} = E_D + 2E_{12} + E_{V_M'''} + 4E_{h^{\cdot}} + \tfrac{2}{3}E_L \tag{4}$$

where E_L is the lattice energy of the oxide M_2O_3. The calculated values of $E_{ox}^{V_M'''}$ are 1044 and 1208 kJ·mol^{-1} for α-Fe_2O_3 and α-Cr_2O_3, respectively.

It is clear that vacancy compensation is by far the most energetically favorable process, as indeed would be expected in view of our prediction of the dominance of Schottky disorder. However, the high value calculated of the energy of oxidation will lead to a very narrow stoichiometry range for the oxidized material. This is in agreement with the findings of Grescovich[27] and Hay *et al.*[28] Of greater interest are the values of the reaction energies of vacancy and hole concentrations with the pressure of oxygen. At lower p_{O_2}, where the material behaves as an intrinsic semiconductor, the hole concentration and hence the electrical conductance will be independent of p_{O_2} with the hole concentration $[h^{\cdot}]$ being governed by the magnitude of the band gap, E_B, as

$$[h^{\cdot}] \propto \exp(-E_B/2kT) \tag{5}$$

The vacancy concentration within this pressure regime can be written using Eq. (3) to give the expression

$$[V_M'''] = \frac{Kp_{O_2}^{3/4}}{[h^{\cdot}]^3} \tag{6}$$

where K is the equilibrium constant for the redox reaction, and will hence have an exponential dependence on the energy of oxidation, i.e.

$$K \propto \exp(-3E_{ox}^{V_M'''}/4) \tag{7}$$

Thus, substituting Eqs. (5) and (7) into Eq. (6) we have

$$V_M''' \propto p_{O_2}^{3/4} \exp\left[\frac{-(\frac{3}{4}E_{ox}^{V_M'''} - \frac{3}{2}E_B)}{kT}\right] \tag{8}$$

The energy term in the exponential is an "effective" formation energy for the defect, which is calculated as 454 kJ·mol^{-1} for α-Fe_2O_3 and 387 kJ·mol^{-1} for α-Cr_2O_3 within the pressure regime where vacancy concentration has a dependence on oxygen partial pressure of $p_{O_2}^{3/4}$. Because of the uncertainties in the calculated band gaps, the experimental values were used in making these estimates and those which follow below.

At higher p_{O_2} it is possible that the hole concentration will be controlled by the deviation from stoichiometry, where we have

$$3[V_M'''] = [h^{\cdot}] \tag{9}$$

Substituting the above equation into Eq. (6), we can write the following expression:

$$[V_M''']^4 = \frac{Kp_{O_2}^{3/4}}{27} \tag{10}$$

Thus we have

$$[V_M'''] \propto K^{1/4} p_{O_2}^{3/16} \tag{11}$$

which gives

$$[V_M'''] \propto \exp\left(\frac{-\frac{3}{16}E_{ox}^{V_M'''}}{kT}\right) p_{O_2} \tag{12}$$

Our effective vacancy formation energies which we equate to $-\frac{3}{16}E_{ox}^{V_M'''}$ in this pressure regime are obtained as 193 and 222 kJ·mol^{-1} for α-Fe_2O_3 and α-Cr_2O_3, respectively.

There is at present little experimental data with which to compare these predictions. In the case of α-Fe_2O_3 there is apparently no evidence for a *p*-type region with cation diffusion via a vacancy mechanism. In contrast for α-Cr_2O_3 there does appear to be at high oxygen pressure *p*-type behavior with cation deficiency. Since our calculated most favorable vacancy migration energy is 204 kJ·mol^{-1} for α-Cr_2O_3, we would predict an Arrhenius energy of 590 kJ·mol^{-1} for the $p_{O_2}^{3/4}$ region and 425 kJ·mol^{-1} for the p_{O_2} region. The calculated results are in reasonable agreement with available experimental Arrhenius energies,[3,7,29] which are in the range 483 to 590 kJ·mol^{-1}.

(2) Defect Structure and Energies in Reduced Materials

Reduction occurs by the formation of electron polaron species with charge compensation by either oxygen vacancies or cation interstitials, either trivalent or divalent. In the former case we have the reaction

$$2O_O^{\times} \rightarrow 2V_O^{\cdot\cdot} + 4e' + O_2 \tag{13}$$

where e' is an electron in the conduction band and for which the energy of reduction ($E_{red}^{V_O^{\cdot\cdot}}$) is

$$E_{red}^{V_O^{\cdot\cdot}} = 2E_{V_O^{\cdot\cdot}} + 4E_{e'} - E_D - 2E_{12} \tag{14}$$

from which values of 1111 and 976 kJ·mol^{-1} for α-Fe_2O_3 and α-Cr_2O_3, respectively, are obtained.

For cation interstitial compensation we have the reactions

$$\tfrac{2}{3}M_2O_3 \rightarrow \tfrac{4}{3}M_i^{\cdot\cdot\cdot} + 4e' + O_2 \tag{15}$$

which applies for trivalent interstitials, and

$$\tfrac{2}{3}M_2O_3 \rightarrow \tfrac{4}{3}M_i^{\cdot\cdot} + \tfrac{8}{3}e' + O_2 \tag{16}$$

for the case of divalent cation interstitials and which yield the following expressions for the reduction energies:

$$E_{red}^{M_i^{\cdot\cdot\cdot}} = -\tfrac{2}{3}E_L + \tfrac{4}{3}E_M + 4E_{e'} - E_D - 2E_{12} \tag{17}$$

$$E_{red}^{M_i^{\cdot\cdot}} = -\tfrac{2}{3}E_L + \tfrac{4}{3}E_M + \tfrac{8}{3}E_{e'} - E_D - 2E_{12} - \tfrac{4}{3}I_3 \tag{18}$$

where I_3 is the third ionization energy of the metal. The expressions give for the case of the trivalent interstitials 1247 and 1217 kJ·mol^{-1} for α-Fe_2O_3 and for α-Cr_2O_3, respectively. For the divalent interstitial we obtain 986 kJ·mol^{-1} for α-Fe_2O_3 and 865 kJ·mol^{-1} for α-Cr_2O_3, suggesting that divalent cations will be the dominant interstitial species.

The energies of reduction with compensation by vacancies and the two types of interstitial species are therefore found to be similar, suggesting a complex defect structure for the reduced material in which all these defect species are present.

In deriving "effective" defect formation energies we again consider two oxygen pressure regimes. At higher p_{O_2} where the composition will be close to stoichiometric the electron concentration will be dominated by the intrinsic semiconducting properties, i.e.

$$[e'] = [h^{\cdot}] \tag{19}$$

Now, using Eq. (15) we have for the concentration of M^{3+} interstitials

$$[M_i^{\cdots}] = \frac{K p_{O_2}^{-3/4}}{[e']^3} \tag{20}$$

where

$$K \propto \exp\left(\frac{-\frac{3}{4}E_{red}^{M_i^{\cdots}}}{kT}\right) \tag{21}$$

and

$$[e'] \propto \exp(-E_B/2kT) \tag{22}$$

Therefore, we have

$$[M_i^{\cdots}] \propto \exp\left[\frac{-(\frac{3}{4}E_{red}^{M_i^{\cdots}} - \frac{3}{2}E_B)}{kT}\right] p_{O_2}^{-3/4} \tag{23}$$

The energy term in the exponential is, as before, the effective defect formation energy for the M^{3+} interstitial. In this pressure regime these are calculated as 604 and 488 kJ·mol^{-1} for α-Fe_2O_3 and α-Cr_2O_3, respectively. Thus we would predict an Arrhenius energy of 792 kJ·mol^{-1} for Fe^{3+} interstitial diffusion in this regime as our lowest activation energy for interstitial motion is 193 kJ·mol^{-1}.

To obtain effective formation energies for the M^{2+} interstitial, we use Eq. (16), which gives

$$[M_i^{\cdot\cdot}] = \frac{K p_{O_2}^{-3/4}}{[e']^2} \tag{24}$$

giving

$$[M_i^{\cdot\cdot}] \propto \exp\left[\frac{-(\frac{3}{4}E_{red}^{M_i^{\cdot\cdot}} - E_B)}{kT}\right] p_{O_2}^{3/4} \tag{25}$$

which gives for the effective formation energy of an Fe^{2+} interstitial in α-Fe_2O_3 a value of 517 kJ·mol^{-1}, while for a Cr^{2+} interstitial in α-Cr_2O_3 we obtain 301 kJ·mol^{-1}.

The anion vacancy concentration is governed by Eq. (13), i.e.

$$[V_O^{\cdot\cdot}] = \frac{K p_{O_2}^{-1/2}}{[e']^2} \tag{26}$$

where

$$k \propto \exp\left(\frac{-\frac{1}{2}E_{red}^{V_O^{\cdot\cdot}}}{kT}\right) \tag{27}$$

Therefore

$$[V_O^{\cdot\cdot}] \propto \exp\left[\frac{-(\frac{1}{2}E_{red}^{V_O^{\cdot\cdot}} - E_B)}{kT}\right] p_{O_2}^{-1/2} \tag{28}$$

giving 333 and 140 kJ·mol^{-1} for the effective vacancy formation energy in α-Fe_2O_3 and α-Cr_2O_3, respectively. When combined with the most favored vacancy migration energies (via the A3 mechanism) these yield estimated Arrhenius energies of 551 and 348 kJ·mol^{-1} for α-Fe_2O_3 and α-Cr_2O_3, respectively.

We must now consider the alternative lower pressure regime in which the electron concentration is determined by the deviation from stoichiometry. Thus if we assume the dominance of M^{3+} interstitials, we have

$$3[M_i^{\cdots}] = [e'] \tag{29}$$

Substituting this into Eq. (15), we have

$$[M_i^{\cdots}]^{16/3} \propto K' p_{O_2} \tag{30}$$

where

$$K' \propto \exp(-E_{red}^{M_i^{\cdots}}/kT) \tag{31}$$

Therefore

$$[M_i^{\cdots}] \propto \exp\left(\frac{\frac{3}{16}E_{red}^{M_i^{\cdots}}}{kT}\right) p_{O_2}^{-3/16} \tag{32}$$

which gives 233 and 228 kJ·mol^{-1} for the effective formation energy of the M^{3+} interstitial in α-Fe_2O_3 and α-Cr_2O_3, respectively. Thus the effective migration energy for M_i in α-Fe_2O_3 is predicted to be 426 kJ·mol^{-1}.

For the M^{2+} interstitial we use Eq. (16), and the same approach as above, which gives

$$[M_i^{\cdot\cdot}] \propto \exp\left(\frac{-\frac{1}{4}E_{red}^{M_i^{\cdot\cdot}}}{kT}\right) p_{O_2}^{-1/4} \tag{33}$$

from which we obtain 246 and 217 kJ·mol^{-1} for the effective formation energies of M^{2+} interstitials in α-Fe_2O_3 and α-Cr_2O_3, respectively.

For the effective formation energy of an oxygen vacancy when interstitials are dominant, we use Eq. (13), together with Eqs. (29) and (32), to give

$$[V_O^{\cdot\cdot}] \propto \exp\left[\frac{-(\frac{1}{2}E_{red}^{V_O^{\cdot\cdot}} - \frac{3}{8}E_{red}^{M_i^{\cdots}})}{kT}\right] p_{O_2}^{-1/8} \tag{34}$$

giving, for the effective vacancy formation energies, values of 88 and 32 kJ·mol^{-1} for α-Fe_2O_3 and α-Cr_2O_3, respectively.

For the case of vacancy predominance we have the electroneutrality condition:

$$2[V_O^{\cdot\cdot}] = [e'] \tag{35}$$

which, on substituting into Eq. (13), gives

$$[V_O^{\cdot\cdot}] \propto K^{1/6} p_{O_2}^{-1/6} \tag{36}$$

Therefore

$$[V_O^{\cdot\cdot}] \propto \exp\left(\frac{-\frac{1}{6}E_{red}^{V_O^{\cdot\cdot}}}{kT}\right) p_{O_2}^{1/6} \tag{37}$$

giving for the effective vacancy formation energy values of 186 and 162 kJ·mol^{-1} for α-Fe_2O_3 and α-Cr_2O_3, respectively, which would yield Arrhenius energies for oxygen vacancy migration of 403 and 402 kJ·mol^{-1}, respectively.

For the effective formation energies of the minority interstitials when vacancies are predominant we use Eqs. (15), (16), (35), and (37) to give for the case of M^{3+}

$$[M_i^{\cdots}] \propto \exp\left[\frac{-(\frac{3}{4}E_{red}^{M_i^{\cdots}} - \frac{1}{2}E_{red}^{V_O^{\cdot\cdot}})}{kT}\right] p_{O_2}^{-1/4} \tag{38}$$

This yields values of 379 and 425 kJ·mol^{-1} for α-Fe_2O_3 and α-Cr_2O_3, respectively. Similarly for M^{2+} interstitials we have

$$[M_i^{\cdot\cdot}] \propto \exp\left[\frac{-[\frac{3}{4}E_{red}^{M_i^{\cdot\cdot}} - \frac{1}{3}E_{red}^{V_O^{\cdot\cdot}}]}{kT}\right] p_{O_2}^{5/12} \tag{39}$$

which gives energies of 184 and 160 kJ·mol^{-1} for α-Fe_2O_3 and α-Cr_2O_3, respectively.

V. Conclusions

The main predictions to emerge from this study are as follows:

(1) In both oxides, electron-hole pair formation energies are lower than the energies of formation of the atomistic defects.

(2) Schottky disorder has the lowest formation energy of the atomistic defects and requires ≈387 to 435 kJ·mol^{-1} per defect.

(3) Oxidation energies are high, ≈970 kJ·mol^{-1}, with cation vacancies being formed. Arrhenius energies of ≈387 to 580 kJ·mol^{-1} are calculated for cation diffusion; these give reasonable agreement with experimental values, which for the case of α-Cr_2O_3 are in the range 483 to 580 kJ·mol^{-1}.

(4) Reduction energies are again high, ≈970 kJ·mol^{-1}, with oxygen vacancies and cation interstitials (both divalent and triva-

lent) having rather similar effective formation energies. At higher values of p_{O_2}, where the electron concentration results from the intrinsic semiconducting properties, we predict a cation migration Arrhenius energy of $\approx$773 kJ·mol^{-1} for α-Fe_2O_3, while for anion migration the predicted Arrhenius energies are 551 and 348 kJ·mol^{-1} for α-Fe_2O_3 and α-Cr_2O_3, respectively. In the alternative low-pressure regime the predicted Arrhenius energy for cation migration in α-Fe_2O_3 is 425 kJ·mol^{-1}, while for anion migration we obtain values of 454 kJ·mol^{-1} for both α-Fe_2O_3 and α-Cr_2O_3.

While there may remain some uncertainties in the calculated defect energies for these oxides, our results should provide a useful basis for the analysis of experimental data.

Acknowledgments: J. C. and J. H. are grateful to the National Board for Science and Technology (Ireland) for supporting this work. We are also grateful to the SERC (U.K.) Collaborative Computer Project 5, to Dr. M. Leslie, Daresbury Laboratory, for assistance, and for the contribution of Peter Thirlby to the early stages of this study.

References

[1]R. H. Chang and J. B. Wagner, Jr., "Direct-Current Conductivity and Iron Tracer Diffusion in Hematite at High Temperatures," *J. Am. Ceram. Soc.*, **55** [4] 211–13 (1972).
[2]R. Dieckmann; private communication to N. L. Peterson.
[3]K. Hoshino and N. L. Peterson, "Cation Self-Diffusion and the Isotope Effect in Fe_2O_3," *J. Phys. Chem. Solids*, **46**, 375–82 (1985).
[4]K. Hoshino and N. L. Peterson, "Cation Self-Diffusion and Impurity Diffusion in Fe_2O_3," *J. Phys. Chem. Solids*, **46**, 1247–54 (1985).
[5]A. Atkinson and R. I. Taylor, "Diffusion of ^{55}Fe in Fe_2O_3 Single Crystals," *J. Phys. Chem. Solids*, **46**, 469–75 (1985).
[6]P. Koftstad; in Nonstoichiometry, Diffusion and Electrical Conductivity in Binary Metal Oxides. Wiley-Interscience, New York, 1982.
[7]A. Atkinson and R. I. Taylor, "Diffusion of ^{51}Cr Tracer in Cr_2O_3 and the Growth of Cr_2O_3 Films"; in Transport in Non-Stoichiometric Compounds. Edited by V. S. Stubican and G. Simkovich. Plenum, New York, 1985.
[8]C. R. A. Catlow, W. C. Mackrodt, M. J. Norgett, and A. M. Stoneham, "The Basic Atomic Processes of Corrosion I. Electronic Conduction in MnO, CoO and NiO," *Philos. Mag. A*, **35**, 177–87 (1977).
[9]C. R. A. Catalow, W. C. Mackrodt, M. J. Norgett, and A. M. Stoneham, "The Basic Atomic Processes of Corrosion II. Defect Structures and Cation Transport in Transition-Metal Oxides," *Philos. Mag. A*, **40**, 161–72 (1979).
[10]C. R. A. Catlow and D. G. Muxworthy, "The Electronic Structure of Divalent Transition Metal Oxides," *Philos. Mag. B*, **37**, 63–71 (1978).
[11]C. R. A. Catlow and R. James, "Disorder in TiO_{2-x}," *Proc. R. Soc. London, Ser. A*, **384**, 157–73 (1982).
[12]N. F. Mott and M. J. Littleton, "Conduction in Polar Crystals I. Electrolytic Conduction in Solid Salts," *Trans. Faraday Soc.*, **34**, 485–99 (1938).
[13]C. R. A. Catlow, R. James, W. C. Mackrodt, and R. F. Stewart, "Defect Energies in α-Al_2O_3 and Rutile TiO_2," *Phys. Rev. B*, **25**, 1006–26 (1982).
[14]M. Leslie, "Program CASCADE: Description of Data Sets for Use in Crystal Defect Calculations," SERC Daresbury Report DL/SCI/TM31T, 1982.
[15]C. R. A. Catlow, "Computer Modelling of Ionic Crystals," *J. Phys. Paris, Suppl.*, **41** [7] C6-53–C6-60 (1980).
[16]R. W. G. Wyckoff, Crystal Structures, 2nd ed., Vol. II. Interscience, New York, 1963.
[17]B. G. Dick and A. W. Overhauser, "Theory of the Dielectic Constants of Alkali Halide Crystals," *Phys. Rev.*, **112**, 90–103 (1958).
[18]W. C. Mackrodt and R. F. Stewart, "Defect Properties of Ionic Solids: II. Point Defect Energies Based on Modified Electron-Gas Potentials," *J. Phys. C*, **12**, 431–49 (1979).
[19]E. Clementi, Tables of Atomic Functions, *IBM J. Res. Dev. Suppl.*, **9** (1965).
[20]K. F. Young and H. P. R. Frederikse, "Compilation of Static Dielectric Constants," *J. Phys. Chem. Ref. Data*, **2**, 313–409 (1973).
[21]G. V. Samsonov, The Oxide Handbook. Plenum, New York, 1982; p. 228.
[22]R. James, "Disorder and Non-Stoichiometry in Rutile and Corundum-Structured Metal Oxides"; Ph.D. Thesis. University of London, 1979, and A.E.R.E. (Harwell) Report T.P. 814, 1979.
[23]W. C. Mackrodt, "Defect Energetics and Their Relation to Non-Stoichiometry in Oxides," *Solid State Ionics*, **12**, 175–88 (1984).
[24]D. Benjelloun, J.-P. Bonnet, and M. Onillon, "Anisotropy of Electrical Properties in Pure and Doped α-Fe_2O_3"; in Transport in Non-Stoichiometric Compounds. Edited by V. S. Stubican and G. Simkovich. Plenum, New York, 1985.
[25]E. W. A. Young, H. Geretsen, and H. J. W. de Wit; private communication.
[26]L. E. Orgel, An Introduction to Transition Metal Chemistry: Ligand Field Theory. Methuen, London, 1960.
[27]C. Grescovich, "Deviation from Stoichiometry in Cr_2O_3 at High Oxygen Partial Pressures," *J. Am. Ceram. Soc.*, **67** [6] C-111–C-112 (1984).
[28]K. A. Hay, S. G. Hicks, and D. R. Holmes, "The Transport Properties and Defect Structure of $(Fe,Cr)_2O_3$ Formed on Fe-Cr Alloys," *Werkst. Korros.*, **21**, 917–24 (1970).
[29]K. Hosino and N. L. Peterson, "Cation Self-Diffusion in Cr_2O_3," *J. Am. Ceram. Soc.*, **66** [11] C-202–C-203 (1983). □